Experimental Evaluation of Tuned Chamber Core Panels for Payload Fairing Noise Control

Noah H. Schiller
Albert R. Allen
NASA Langley Research Center, Hampton VA
Jonathan W. Herlan
University of Mississippi, Oxford MS
Bruce N. Rosenthal
NASA Glenn Research Center, Cleveland OH

ABSTRACT

Analytical models have been developed to predict the sound absorption and sound transmission loss of tuned chamber core panels. The panels are constructed of two facesheets sandwiching a corrugated core. When ports are introduced through one facesheet, the long chambers within the core can be used as an array of low-frequency acoustic resonators. To evaluate the accuracy of the analytical models, absorption and sound transmission loss tests were performed on flat panels. Measurements show that the acoustic resonators embedded in the panels improve both the absorption and transmission loss of the sandwich structure at frequencies near the natural frequency of the resonators. Analytical predictions for absorption closely match measured data. However, transmission loss predictions miss important features observed in the measurements. This suggests that higher-fidelity analytical or numerical models will be needed to supplement transmission loss predictions in the future.

KEY WORDS: Acoustic, resonators, tuned, chamber, core, impedance, absorption, transmission loss, noise reduction

NOMENCLATURE

Symbols

A	= absorption area, m^2	$\hat{p}$	= complex pressure amplitude, Pa
α	= ratio of inlet areas to panel area	ψ	= angle between x-axis and projection of incident wave on xy plane, rad
c	= ambient speed of sound, m/s	R	= acoustic resistance, $kg/(m^2s)$
D	= bending stiffness, $kg\ m^2/s^2$	r	= radius of the inlet, m
f	= frequency, Hz	ρ	= ambient fluid density, kg/m^3
IL	= insertion loss, dB	S	= surface area, m^2
j	= $\sqrt{-1}$	SPL	= sound pressure level, dB
k	= acoustic wavenumber, rad/m	σ	= radiation efficiency
L	= effective length, m	TL	= transmission loss, dB
λ	= wavelength, m	τ	= transmission coefficient
m_s	= mass per unit area, kg/m^2	θ	= angle of incidence from plate normal, rad
M	= acoustic inertance, kg/m^4	v	= transverse velocity of panel, m/s

N	= number of resonators	W	= sound power, kg m^2/s^3
NR	= noise reduction, dB	Z	= specific impedance, kg/(m^2s)
ω	= radial frequency, rad/s		

Subscripts and Superscripts

b	= baseline	m	= index
c	= cavity	n	= neck
d	= diffuse field	rad	= radiation
ext	= exterior	r	= resonator
f	= fluid or finite	ri	= resonator input
i	= inlet or incident	t	= transmitted
int	= interior	x	= X-direction
p	= panel	y	= Y-direction

INTRODUCTION

NASA's new Space Launch System (SLS) will generate unprecedented thrust at liftoff. This will enable the vehicle to lift larger payloads than any other rocket; however, the extra thrust will also generate high acoustic levels, which have the potential to damage sensitive equipment in the payload bay. While conventional porous treatment can be used to mitigate high-frequency noise inside the payload fairing, low-frequency noise is difficult to attenuate without using thick, heavy treatment. Acoustic resonators can be used as an alternative to porous treatment for low-frequency sound mitigation, however add-on resonators necessarily take up space and add weight to the structure. Minimizing these two parameters is very important, particularly in aerospace applications. Researchers from the Air Force Research Laboratory previously proposed a minimal-weight noise control solution for launch vehicle applications (Lane et al. 2005, Lane et al. 2007). They considered a double-wall fairing with long rectangular chambers sandwiched between inner and outer facesheets. Ports were added to the inner facesheet to couple the chambers, or resonators, to the interior payload bay. A 1.51 m diameter cylindrical test article was built to evaluate the concept. The test article contained embedded resonators tuned to frequencies ranging from 60 to 2,000 Hz. They found that the noise reduction, or difference between the average sound pressure outside and inside the cylinder, increased significantly when the resonators were active. Li and Vipperman performed a thorough experimental characterization of a similar structure and also showed promising results in terms of noise reduction (Li and Vipperman, 2006).

Based on the promising results of Lane et al. and Li and Vipperman, a similar concept referred to as a Tuned Chamber Core (TCC) structure has been studied at NASA (Schiller et al. 2014, Allen et al. 2014). While earlier concepts contained rectangular chambers within the core, the TCC structure has two facesheets sandwiching a corrugated core, as shown in Figure 1. When ports are introduced through one facesheet, the long chambers within the core can be used as an array of low-frequency acoustic resonators. The embedded resonators have the potential to reduce interior noise without increasing the weight or size of the structure. It is useful to note that corrugated sandwich structures are currently used in aerospace, automotive, rail, shipbuilding, and building construction applications because they can have a very high stiffness-to-weight ratio (Chang et al. 2005). Therefore, it is possible that significant acoustic benefits could be realized in many of these same applications with relatively minor modifications to the structure.

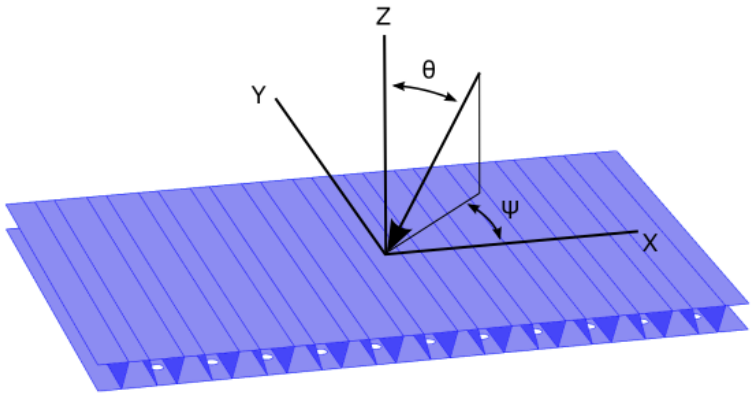

Figure 1: Tuned chamber core panel with trapezoidal core, and inlets/ports in the bottom facesheet. The coordinate system used for the analysis is also shown.

The long term goal of the current study to quantify the benefit of using the TCC concept for new composite launch vehicle structures, such as a large diameter payload fairing. Since large structures could contain thousands of resonators, it is not practical to explicitly model each resonator within a large finite element model. Instead, this work focuses on the development and evaluation of computationally-efficient analytical models that capture the effect of the embedded resonators.

This paper begins with a description of the analytical models. The testing performed to assess the accuracy and usefulness of the models is then described. Specifically, descriptions of the test articles, facility, and measurement procedure are provided. A comparison of the analytical predictions and panel-level measurements are then presented and finally, some concluding remarks are provided.

ANALYTICAL MODELS

The performance of acoustic treatment is often quantified in terms of noise reduction, which is the difference between the exterior and interior sound pressure levels. Assuming steady-state conditions, the exterior and interior sound fields are diffuse, and the interior is lightly damped, then the noise reduction can be approximated as

$$NR = SPL_{ext} - SPL_{int} \approx 10 \log_{10}\left(\frac{A_{int}}{S_{int}}\right) + TL_d \qquad (1)$$

where A_{int} is the absorption area of the interior acoustic space, S_{int} is the interior surface area, and TL_d is the diffuse field transmission loss. Notice that the noise reduction depends on the interior absorption of the payload bay as well as the transmission loss through the fairing. So to fully understand the effect of the embedded resonators, accurate models for both components are needed.

An impedance representation for the resonators is described first. Representing the embedded resonators as an equivalent surface impedance enables the development of the computationally-efficient analytical models. Following the impedance discussion, absorption and transmission loss models that are based on the impedance representation will be presented.

Impedance representation for embedded resonators

The resonators embedded within the corrugated-core panel consist of long trapezoidal cavities with an inlet near one end. The fact that the inlet is in the side of the cavity, and not at the end, makes little difference at low frequencies (Cummings 1975). Therefore the input impedance of the resonators can be estimated by combining the impedance of a long cavity with the impedance of the inlet. Based on a plane-wave analysis, the specific acoustic impedance of a cavity with a rigid back wall, as seen from the inlet, can be written as (Panton and Miller 1975):

$$Z_c = -j\frac{\rho c}{S_c}\cot(kL_c)S_i \tag{2}$$

where ρ is the density of the fluid, c is the speed of sound, S_c is the cross-sectional area of the cavity, $k = \omega/c$ is the wavenumber, L_c is the length of the cavity, and S_i is the cross-sectional area of the inlet. If losses are neglected, the specific acoustic impedance of the inlet can be represented as (Panton and Miller 1975)

$$Z_i = j\omega M_i S_i \tag{3}$$

where $M_i = \rho L_n/S_i$ is the acoustic inertance of the fluid in the neck of the inlet, and L_n is the effective length of the neck. The effective length of the neck equals the thickness of the facesheet plus an additional $8r/(3\pi)$ interior end correction term to account for the internal fluid loading, where r is the radius of the circular inlet (Kinsler et al. 2000). The combined specific acoustic input impedance of the resonator can then be expressed as

$$Z_{ri} = Z_i + Z_c = jk\rho c L_n - j\frac{\rho c}{S_c}\cot(kL_c)S_i + R \tag{4}$$

where *R* is a resistance term that accounts for the thermal and viscous losses in the cavity and inlet. This term affects the quality factor of the resonator.

The input impedance of the resonator is important, however it is also necessary to account for the radiation impedance of the acoustic wave propagated away from the resonator. Since the inlet is circular, the radiation impedance for a baffled circular piston can be used to approximate the radiation impedance. At low frequencies, where $kr \ll 1$, the specific acoustic radiation impedance can be approximated as (Kinsler et al. 2000)

$$Z_{rad} = j\rho ckr\,8/(3\pi) + \rho c(kr)^2/2 \tag{5}$$

The imaginary part of Eqn. (5) essentially represents a mass loading on the resonator, which decreases the resonance frequency. The real part of Eqn. (5) is an additional loss term accounting for the power radiated into the fluid surrounding the resonator. The total impedance of the resonator coupled to the surrounding fluid can then be written as

$$Z_r = Z_{ri} + Z_{rad} \tag{6}$$

Note that this expression was derived for a single isolated resonator. If an array of resonators is considered, and the separation distance between the inlets is less than half a wavelength, then the mutual interaction between neighboring resonators will increase the radiation impedance (Pritchard 1960). This would reduce the natural frequency of the resonators and add damping to the system. However, since the interaction between resonators is expected to be a second order effect, it is not included in the models presented in this paper.

Absorption

Resonators are commonly used to increase the absorption of interior spaces. Performance of the

resonators is typically quantified in terms of the absorption cross-section, which is also referred to as the equivalent absorption area. Absorption area is defined as the power absorbed by the resonator divided by the incident intensity. Near resonance, the absorption area can be much larger than the actual area of the resonator inlet. At low frequencies, where the inlet is small relative to a wavelength, the absorption cross section is independent of the angle of incidence (Ingard 2010). Therefore the effective absorption area for a resonator exposed to a diffuse sound field should equal the absorption area of the same resonator driven by normally incident sound. That expression is commonly cited for a single resonator as (Ingard 2010)

$$A_r^m = 4\rho c S_i \frac{\mathrm{Re}(Z_{ri})}{|Z_{ri} + Z_{rad}|^2} \tag{7}$$

where A_r^m is the effective absorption area of the mth resonator, S_i is the cross-sectional area of the inlet, and $\mathrm{Re}(Z_{ri})$ is the real part of the input impedance (i.e. the input resistance of the resonator).

To analyze the TCC concept, it is necessary to account for multiple resonators arranged in an array. For this analysis, the resonator inlets are assumed to be sufficiently far apart to act independently of each other. Therefore the total diffuse field absorption area of the array can be found by taking the sum of individual absorption cross sections

$$A_r = \sum_m^N A_r^m \tag{8}$$

where N is the number of resonators in the array.

The amount of absorption present in an enclosed acoustic space, such as the payload bay, can have a large impact on the resulting sound pressure level. If assumptions are made similar to the ones used to derive Eqn. (1), then an expression for the change in the interior sound pressure level due to the absorption added by the resonators can be written as

$$\Delta SPL = SPL_b^{int} - SPL_{r+b}^{int} \approx 10\log_{10}\left(\frac{A_r + A_b}{A_b}\right) \tag{9}$$

where SPL_b^{int} is the spatially averaged sound pressure level in a lightly damped interior with a baseline absorption area A_b, and SPL_{r+b}^{int} is the sound pressure level in the interior with additional absorption provided by the resonator array. Clearly, the benefit of the resonators depends on both the baseline absorption area as well as the additional absorption introduced by the resonator array. If the interior space is lightly damped (i.e. A_b is small), then the addition of a relatively small amount of additional absorption will significantly reduce the interior sound pressure level. Conversely, if the space is already heavily damped, then the change in sound pressure level due to the resonator array will be modest. Since the goal is to validate models that capture the effect of the resonator array, the metric used to evaluate the accuracy of the absorption model will be ΔSPL, as defined in Eqn. (9).

Transmission Loss

As Eqn. (1) shows, the noise reduction of an enclosure is dependent on both absorption and transmission loss. Transmission loss is defined as the ratio of the power incident on the outside of the structure to the power radiated into the interior. Since both the interior and exterior sound fields are assumed to be diffuse in this study, the transmission loss defined in Eqn. (1) is the diffuse field sound transmission loss. To model the change in transmission loss due to the resonators, it is

helpful to first consider the oblique incidence sound transmission through a flexible panel with embedded resonators.

When an acoustic plane wave is incident on the panel, the transverse velocity of the structure can be written as

$$v = \frac{2\widehat{p_i}}{Z_p + Z_f + Z_t} \tag{10}$$

where $\widehat{p_i}$ is the complex amplitude of the incident pressure wave, Z_p is the specific surface impedance of the panel, $Z_f = \rho c/\big(\cos(\theta)\big)$ is the local specific impedance of the fluid at the surface of the panel, θ is the propagation angle of the incident pressure wave as depicted in Figure 1, and Z_t is the combined specific acoustic impedance of the fluid and the resonators on the transmitted side. To calculate Z_t the impedances of the fluid and resonators are combined in parallel while taking into account the surface area of each as

$$Z_t = \frac{1}{\frac{1-\alpha}{Z_f} + \frac{\alpha}{Z_r}} \tag{11}$$

where $\alpha = NS_i/S_p$ is the ratio of the total resonator inlet areas divided by the total panel surface area, N is the number of resonators in the panel, and S_p is the surface area of the radiating side of the panel. The relationship between the transmitted acoustic wave and the transverse velocity of the panel can be written as

$$\widehat{p_t} = Z_t v \tag{12}$$

where $\widehat{p_t}$ is the complex amplitude of the transmitted wave. The plane wave sound-power transmission coefficient for an infinite panel can then be defined as

$$\tau(\theta) = \left|\frac{\widehat{p_t}}{\widehat{p_i}}\right|^2 = \left|\frac{2Z_t}{Z_p + Z_f + Z_t}\right|^2 \tag{13}$$

and therefore the plane wave transmission loss is

$$TL(\theta) = 10\log_{10}\big(1/\tau(\theta)\big) = 10\log_{10}\left(\left|\frac{Z_p + Z_f + Z_t}{2Z_t}\right|^2\right) \tag{14}$$

Notice that transmission loss is affected by the impedance of the fluid, resonators, and panel. Since the TCC panels have a corrugated core, the bending stiffness is highly directional. Therefore the surface impedance of the corrugated sandwich panel was approximated using an expression for a thin orthotropic plate, which should be valid at low frequencies. For an infinite orthotropic panel, the specific surface impedance can be written as (Heckl 1960)

$$Z_p = j\omega m_s\left(1 - \frac{D_x k_x^4}{\omega^2 m_s} - \frac{2D_{xy}k_x^2 k_y^2}{\omega^2 m_s} - \frac{D_y k_y^4}{\omega^2 m_s}\right) \tag{15}$$

where m_s is the mass per unit area of the panel, $k_x = k\sin(\theta)\cos(\psi)$, $k_y = k\sin(\theta)\sin(\psi)$, D_x is the bending stiffness in the compliant cross direction, D_y is the bending stiffness in the stiff axial direction, and $D_{xy} = \sqrt{D_x D_y}$.

The previous derivation assumes that the panel is infinite. However, that assumption can result in a significant low frequency error for finite panels (Schiller and Allen 2015). To account for the finite size of the panel, the angle dependent transmission coefficient, shown in Eqn. (13), can be updated to account for the finite panel radiation efficiency as described by (Villot et al. 2001 and

Vigran 2009). The diffuse field transmission coefficient for the finite size panel can then be calculated by integrating the updated plane wave transmission coefficient, $\tau_f(\theta,\psi)$, over all angles of incidence

$$\tau_d = \frac{\int_0^{2\pi}\int_0^{\pi/2}\tau_f(\theta,\psi)\sin(\theta)\cos(\theta)d\theta\, d\psi}{\int_0^{2\pi}\int_0^{\pi/2}\sin(\theta)\cos(\theta)d\theta\, d\psi} \tag{16}$$

Finally, the diffuse field transmission loss can be calculated as

$$TL_d = 10\log_{10}(1/\tau_d) \tag{17}$$

Once again, since the goal is to validate models that capture the effect of the resonators, the metric for the comparison is insertion loss, which is defined as

$$IL = TL_r - TL_b \tag{18}$$

where TL_r is the diffuse field transmission loss of the TCC structure with embedded resonators, and TL_b is the diffuse field transmission loss of the baseline structure without the embedded resonators (i.e. $N = 0$).

TEST SETUP AND MEASUREMENTS

This section describes the TCC test articles as well as the Structural Acoustic Loads and Transmission (SALT) facility where the tests were performed. The measurement procedures used for both the absorption and transmission loss tests are also described.

Test articles

Three nominally identical TCC panels were tested. One of the panels is shown in Figure 2. The panels are 0.81 m long, 1.22 m wide, and 0.051 m thick. The sandwich panels have 1 mm thick facesheets bonded to a corrugated core, both of which are made of carbon fiber. The core is separated into 22 chambers that run the length of the panel. Each chamber is sealed using two closed cell foam plugs that were inserted into the core from the sides of the panel. Holes were drilled in the top facesheet to serve as the inlets for the acoustic resonators. The inlets to each chamber are staggered on either side of the panel. Once built, the panels were experimentally characterized to estimate the effective bending stiffnesses in the X- (width) and Y- (length) directions, as described in the Appendix. The nominal panel properties are shown in Table 1.

Figure 2: Tuned chamber core panel with inlets facing up. The white foam plugs, used to seal the cavities, can be seen in every other chamber. Plugs were inserted deeper into neighboring chambers, and are therefore not visible.

An advantage of using resonators for low-frequency acoustic mitigation is that the performance can be targeted for a desired frequency range. For this test, all resonators were tuned for either 200 Hz or 315 Hz. While the targeted frequencies would likely be lower for the payload fairing application, these particular frequencies were selected because they lie within the operating range of the facility.

To target the desired frequencies, each resonator was tuned by adjusting the position of the foam plug farthest from the inlet. This modified the length of the interior cavity and therefore changed the natural frequency of the resonator. The foam used for these tests was a 32 kg/m^3 density, cross-linked, polyethylene foam. This type of closed-cell foam recovers quickly after compression and was found to provide a good acoustic seal. The position of the plugs was determined using the analytical impedance model previously discussed. If damping is neglected, then resonance corresponds to frequencies where the reactance (i.e. imaginary part of the total impedance given in Eqn. (6)) equals zero

$$\mathrm{Im}(Z_r) = k\rho c L_n - \frac{\rho c}{S_c}\cot(kL_c)S_i + \rho c k r\, 8/(3\pi) = 0 \tag{19}$$

Therefore the first resonance, or natural frequency, of the resonator was estimated by solving Eqn. (19) for L_c

$$L_c = \frac{c}{2\pi f_n}\cot^{-1}\left(\frac{2\pi f_n S_c L_n}{c S_i} + \frac{16 f_n r S_c}{3 c S_i}\right) \tag{20}$$

where f_n is the desired natural frequency. The effective cavity lengths for both the 200 Hz and 315 Hz configurations are shown in Table 1. These lengths correspond to the distance from the edge of the inlet to the far plug.

Table 1 also includes the input resistance of the resonators. This term accounts for loss mechanisms such as wall dissipation in the cavity and inlet losses associated with boundary layer separation or vortex formation. However, it does not account for acoustic radiation, which was modeled separately. The input resistance was empirically determined to be 10 kg/(m^{2}s) using previously collected data described in (Allen et al. 2014).

Table 1: Nominal resonator and panel properties.

Inlet radius, r	0.013 m	Number of embedded resonators, N	22
Inlet cross-section area, S_i	5.1×10^{-4} m^2	Mass per unit area of panel, m_s	4.3 kg/m^2
Cavity cross-sectional area, S_c	2.6×10^{-3} m^2	Panel width in the X-direction, L_x	1.2 m
Effective neck length, L_n	0.012 m	Panel length in the Y-direction, L_y	0.81 m
Effective cavity length, L_c (200 Hz config.)	0.32 m	Bending stiffness in the X-direction, D_x	10 Nm
Effective cavity length, L_c (315 Hz config.)	0.17 m	Bending stiffness in the Y-direction, D_y	10^5 Nm
Resonator input resistance, R	10 kg/(m^{2}s)		

Facility description

The measurements were collected in NASA Langley's Structural Acoustic Loads and Transmission (SALT) facility. The SALT facility consists of a reverberant source room coupled to an anechoic chamber through a window, as shown in Figure 3. The reverberant source room is approximately 9.5 m wide, 6.5 m deep, and 4.5 m tall and includes irregularly splayed walls to disrupt the formation of standing waves at low frequencies. The source room contains 18 high-frequency wall-mounted compression drivers and 4 mid- and low-frequency floor-mounted loudspeakers. A previous characterization of the reverberation chamber showed that the sound field can be treated as approximately diffuse down to 200 Hz (Grosveld 2013). For these tests, a prototype 3.1 m by 1.8 m rotating diffusor was installed in the reverberation room in an effort to improve the diffuse field characteristic of the sound field in a time averaged sense.

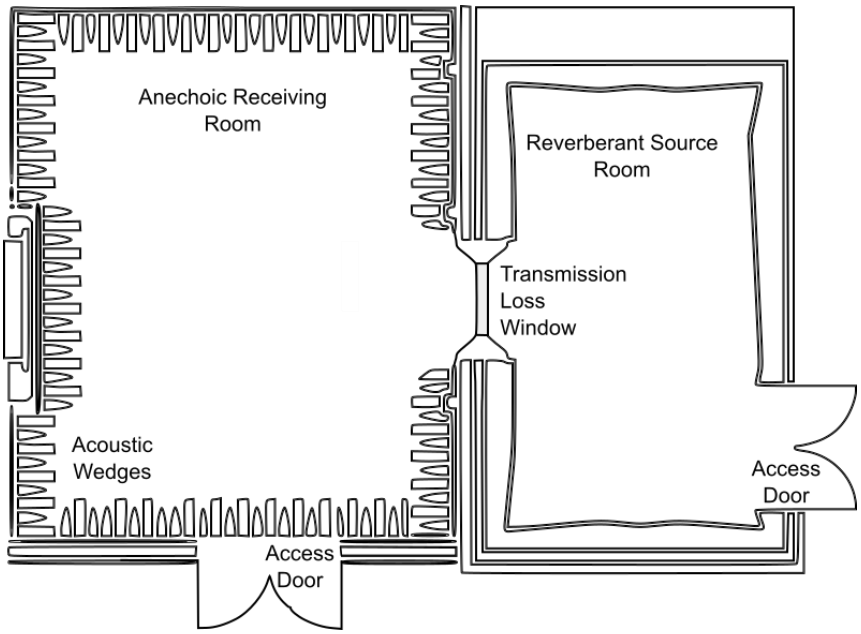

Figure 3: Diagram of the SALT facility.

The anechoic receiving room is approximately 9.63 m wide, 7.65 m deep, and 4.57 m tall and is located adjacent to the reverberant source room. The floor, ceiling, and walls of the room are covered with approximately 4,850 open-cell polyurethane wedges that are each 0.914 m tall. The wedges significantly reduce reflections creating a nearly free-field acoustic environment down to 80 Hz (Grosveld 1999).

The transmission loss window, connecting the source and receiver rooms, can accommodate structures up to 1.41 m by 1.41 m, however smaller panels can also be accommodated by installing an adaptor frame that reduces the size of the opening. Additional details regarding the facility, and its capabilities can be found in (Grosveld 2013) and (Rizzi et al. 2013).

Absorption measurement procedure

The change in absorption due to the resonators was quantified indirectly by measuring the

difference in the spatially averaged sound pressure level in the reverberant test chamber with and without the resonators. This method, as opposed to standard reverberation decay rate techniques, was found to be well suited to resolve the narrowband resonator array characteristics. Since the test only required the reverberation chamber, a heavy panel was installed in the transmission loss window to minimize the energy lost to the anechoic room. The three 1.22 m by 0.81 m test articles were placed adjacent to each other on the floor of the chamber with the inlets facing up. The room was ensonified using 22 uncorrelated acoustic sources, and the spatially averaged sound pressure level was estimated with 12 stationary microphones located throughout the room. The resonator inlets were then sealed using masking tape, and the spatially averaged sound pressure level was again measured. This procedure was repeated 3 times with the test articles placed at different locations on the floor of the reverberation chamber. The average mean square pressure was then calculated for the two separate cases (i.e. inlets open and inlets closed). Finally, the change in sound pressure level due to the resonator array was calculated as the difference between the sound pressure levels with the inlets open (i.e. resonators active) and closed. In order to use a change in sound pressure level to quantify the change in absorption, the power input into the room must be fixed. In these tests, the drive signal spectra used for both the open and closed inlet tests were identically shaped. In addition, since the influence of a reverberant field on a source goes to zero in a time-average sense, the power output from the speakers should have been insensitive to the small changes in room absorption caused by the array of resonators (Jacobsen and Juhl 2013).

To predict the change in sound pressure level measured during the test, it was necessary to know the baseline absorption in the test chamber with the resonators inactive. Therefore an additional test was required to quantify the baseline absorption. This was performed using standard reverberation decay rate methods for measuring sound absorption (ASTM C423). Specifically, band-limited excitation signals were generated for each third-octave band. The signals were sent to the speakers, one at a time, while the room response was measured using the stationary microphones. Average decay times were estimated, and then the absorption area for the chamber was calculated using the Sabine formula.

Transmission loss measurement procedure

The transmission loss tests were performed on one of the 1.22 m by 0.81 m test articles. To mount the panel in the transmission loss window, a wooden adapter frame was built and installed in the window. The perimeter of the adapter was sealed with dense mastic to eliminate leaks and reduce flanking transmission. With the test article installed, the source room was ensonified and the room averaged sound pressure level was determined. The sound power incident on the test article W_i was then inferred from the average sound pressure level in the source room. The surface averaged, transmitted sound intensity was measured using a traversing array of five intensity probes on the receiving room side of the test article. The transmitted sound power W_t was then calculated by multiplying the average transmitted intensity by the measurement surface area. Finally, transmission loss was found as

$$TL = 10\log_{10}(W_i/W_t) \tag{21}$$

This procedure for measuring transmission loss follows the discrete point method described in standard (ASTM E2249).

The transmission loss performance of the resonator array was quantified in terms of insertion loss (Eqn. (18)) by taking the difference between the measured transmission loss with the resonator inlets open and closed. Back-to-back transmission loss tests were performed in this way for both the 200 Hz and 315 Hz panel configurations. Masking tape was again used to cover the inlets for the closed cases.

RESULTS AND DISCUSSION

The accuracy of the absorption model is assessed by comparing ΔSPL, as defined in Eqn. (9), with measurements. Figure 4 shows that both measurements and predictions are positive, indicating that the resonator array reduces the spatially averaged sound pressure level. Around the natural frequency of the resonators, the reductions are on the order of 2-3 dB and the predictions and measurements agree very well, aside from a slight shift in the peak. This offset could be attributed to the mutual interaction between the resonators, which was neglected in the model. The interaction would result in a higher radiation impedance, which would shift the prediction to the left.

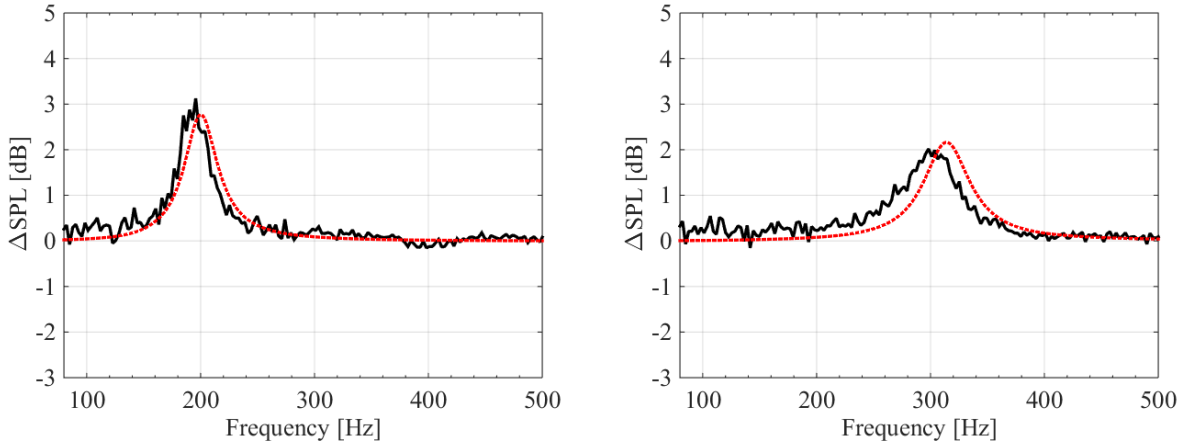

Figure 4: Predicted (▪▪▪) and measured (▬) change in sound pressure level in the reverberation chamber due to the 200 Hz (left) and 315 Hz (right) tuned resonator arrays.

Recall from Eqn. (8) that the absorption area of the array depends on the number of resonators. This test was performed with 66 resonators (3 panels with 22 resonators each) while a large payload fairing could contain thousands of resonators embedded in the structure. Therefore, the 2-3 dB reductions demonstrated in these tests are not necessarily representative of the reductions one could achieve in a full-scale system.

Figure 5 compares insertion loss measurements and predictions (Eqn. (18)) for both the 200 Hz and 315 Hz configurations. Recall that insertion loss is defined as the change in transmission loss due to the resonators. In this case, positive values are indicative of an increase in transmission loss due to the resonators. Both the measurements and predictions show that the embedded resonators provide some benefit around resonance. However, the predictions do not capture other measurement trends. Specifically, the predictions do not capture the region just below resonance where the insertion loss is negative. Given this discrepancy, it is suggested that higher-fidelity

numerical models be used in addition to the analytical model when predicting the sound transmission performance of TCC or similar structures.

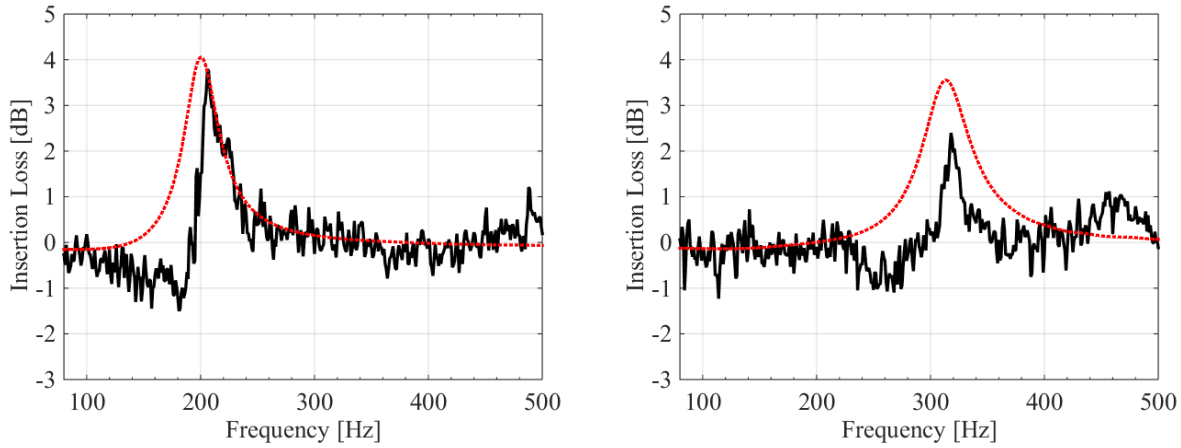

Figure 5: Predicted (▪▪▪) and measured (—) insertion loss due to the 200 Hz (left) and 315 Hz (right) tuned resonator arrays.

Unlike absorption, the insertion loss is not expected to improve significantly when evaluated using larger test articles. This is because insertion loss is determined by the number of resonators per unit area (Schiller et al. 2014), and not the total number of resonators installed in the structure. Therefore, the majority of the benefit for the payload fairing application would come from the change in low frequency absorption. Regardless, the fact that the resonators provide some benefit in terms of low frequency transmission loss is noteworthy.

CONCLUDING REMARKS

Analytical models were developed to predict the effect of acoustic resonators embedded in chamber core panels. Model accuracy was assessed by comparing predictions with measurements acquired using flat, tuned chamber core panels. Measurements showed that the acoustic resonators improved both the absorption and sound transmission loss of the sandwich structure at frequencies near the natural frequency of the resonators. The absorption predictions closely matched measurements, indicating that the analytical models are sufficient for future absorption predictions. In contrast, there were some differences between transmission loss predictions and measurements. The model over predicted the benefit of the resonator array on transmission loss, and missed important trends seen in the measurements. Therefore, future transmission loss predictions should be supplemented with higher-fidelity models. Future work will focus on validating integrated models of larger, more realistic tuned chamber core systems.

ACKNOWLEDGEMENTS

The authors gratefully acknowledge the support of the Payload Fairing Team, including Joe Roche, Bart Zalewski, Cameron Cunningham, Tom Krivanek, Paul Senick, Anne McNelis, Bill Hughes, and Dan Kosareo. The authors are also grateful to Justin Jackson for his role in panel fabrication.

REFERENCES

Allen A. R., Schiller, N. H., Zalewski, B. F., and Rosenthal, B. N., "Transmission Loss and Absorption of Corrugated Core Sandwich Panels with Embedded Resonators," *in Proceedings of Noise-Con*, (2014).

ASTM C423-09a, "Standard Test Method for Sound Absorption and Sound Absorption Coefficients by the Reverberation Room Method," (2009).

ASTM E90-09, "Standard Test Method for Laboratory Measurement of Airborne Sound Transmission Loss of Building Partitions and Elements," (2009).

Chang, W. S., Ventsel, E., Krauthammer, T., and John, J., "Bending Behavior of Corrugated-Core Sandwich Plates," *Composite Structures* 70, no. 1 (2005): 81-89.

Cummings, A., "Sound Transmission in 180 Degree Duct Bends of Rectangular Section," *Journal of Sound and Vibration* 41, no. 3 (1975): 321-334.

Fahy, F., and Gardonio, P., *Sound and Structural Vibration: Radiation, Transmission, and Response, 2nd Edition*, Academic Press, (2007).

Ingard, U., *Noise Reduction Analysis*, Jones and Bartlett Publishers, (2010).

Heckl, M. "Untersuchungen an Orthotropen Platten" *Acta Acustica united with Acustica* 10, no. 2 (1960): 109-115.

Jacobsen, F., and Juhl, P. M., *Fundamentals of General Linear Acoustics*, Wiley, (2013).

Kinsler, L. E., Frey, A. R., Coppens, A. B., & Sanders, J. V., *Fundamentals of Acoustics, 4th Edition*, John Wiley & Sons, (2000).

Lane, S. A., Henderson, K., Williams, A., and Ardelean, E., "Chamber Core Structures for Fairing Acoustic Mitigation," *Journal of Spacecraft and Rockets* 44, no. 1 (2007): 156-163.

Lane, S. A., Richard, R. E., & Kennedy, S. J., "Fairing Noise Control using Tube-Shaped Resonators," *Journal of Spacecraft and Rockets* 42, no. 4, (2005): 640-646.

Li, D., and Vipperman, J. S., "Noise Control of Mock-Scale Chambercore Payload Fairing using Integrated Acoustic Resonators," *Journal of Spacecraft and Rockets* 43 no. 4, (2006): 877-882.

Panton, R. L., and Miller, J. M., "Resonant Frequencies of Cylindrical Helmholtz Resonators," *Journal of the Acoustical Society of America* 57, no. 6, (1975): 1533-1535.

Pritchard R. L., "Mutual Acoustic Impedance between Radiations in an Infinite Rigid Plane," *Journal of the Acoustical Society of America* 32, no. 6, (1960): 730-737.

Schiller, N. H., and Allen, A. R., "Assessment of Analytical Predictions for Diffuse Field Sound Transmission Loss," *in Proceedings of InterNoise*, (2015).

Schiller, N. H., Allen, A. R., Zalewski, B. F., and Beck, B. S., "Sound Transmission Loss through a Corrugated-Core Sandwich Panel with Integrated Acoustic Resonators," *in Proceedings of ASME IMECE*, (2014).

Vigran T. E., "Predicting the Sound Reduction Index of Finite Size Specimen by a Simplified Spatial Windowing Technique," *Journal of Sound and Vibration* 325, (2009).

Villot M., Guigou C., and Gagliardini L., "Predicting the Acoustical Radiation of Finite Size Multi-Layered Structures by Applying Spatial Windowing on Infinite Structures," *Journal of Sound and Vibration* 245, (2001).

APPENDIX: EXPERIMENTAL ESTIMATE OF PLATE BENDING STIFFNESSES

Effective plate bending stiffnesses of the TCC test panel were estimated by measuring the apparent wavelengths in the axial- and cross-corrugation directions. This measurement involved supporting the panel in an approximately free boundary condition using bungee cords, exciting the panel with band-limited noise using a shaker, and measuring the normal response with a scanning laser vibrometer. Scans were performed at a resolution of 19 mm along orthogonal lines spanning 1.120 m and 0.727 m in the cross- and axial-corrugation directions, respectively. The resulting data set included normal velocity frequency response functions referenced to the pseudo-random drive signal voltage at each point in the scan lines. Frequencies up to 1 kHz were considered to envelope the selected resonances of the TCC panel embedded resonators.

Typically, a spatial Fourier transform post processing procedure can be used to estimate the frequency dependent wavelengths given a measured velocity field. This is an effective method when multiple wavelengths occur within the range of the field, but fails when only one wavelength or less is available. Because the TCC test article exhibited wavelengths on the order of the panel extent or less in the frequency range considered, especially in the stiff axial direction, a nonlinear regression technique was adopted. The measured data was assumed to fit the sinusoidal model

$$y = s_1 \sin(s_2 x + s_3) + s_4 \tag{22}$$

where s_1-s_4 represent the amplitude, wavenumber, phase, and bias of the underlying waveform y sampled at locations x. The squared error relative to the measured waveform y_m was formulated as

$$\varepsilon = (y - y_m)^2 \tag{23}$$

and minimized using the Nelder-Mead Simplex algorithm within Matlab's *fminsearch*. This procedure was performed at the observable panel resonance frequencies below 1 kHz and obviously poor fits were removed from the results. The resulting wavelength estimates ($\lambda = 2\pi/s_2$) are shown in Figure 6. Lines representing the free flexural wavelengths of an equivalent plate given by

$$\lambda = \frac{2\pi}{(\omega^2 m/D)^{1/4}} \tag{24}$$

are also shown with first order approximations of the plate bending stiffness $D = 10$ Nm and 10^5 Nm for the cross- and axial-corrugation directions, respectively.

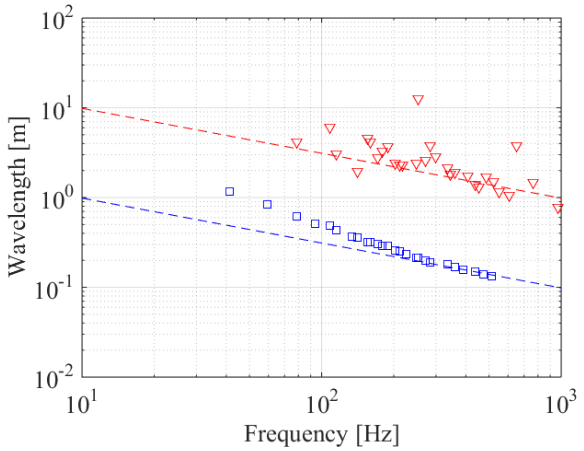

Figure 6: Apparent wavelengths of the TCC in the cross- and axial-corrugation directions (□, ▽) estimated from corresponding normal velocity line measurements. Free flexural wavelengths of an equivalent plate with flexural stiffness D = 10 Nm and 1E5 Nm (– –, – –) are also shown.